THE JOURNAL OF PHYSICAL CHEMISTRY C
A JOURNAL OF THE AMERICAN CHEMICAL SOCIETY

pubs.acs.org/JPCC

Article

Quantification of Hydride Coverage on Cu(111) by Electrochemical Mass Spectrometry

David Raciti* and Thomas P. Moffat*

Cite This: J. Phys. Chem. C 2022, 126, 18734−18743

Read Online

ACCESS | Metrics & More | Article Recommendations | Supporting Information

ABSTRACT: Electrochemical mass spectrometry (EC-MS) is combined with chronoamperometry to quantify H coverage associated with the surface hydride phase on Cu(111) in 0.1 mol/L H_2SO_4. A two-step potential pulse program is used to examine anion desorption and hydride formation, and the inverse, by tracking the 2 atomic mass unit (amu) signal for H_2 production in comparison to the charge passed. On the negative potential step, the reduction current is partitioned between anion desorption, hydride formation, and the hydrogen evolution reaction (HER). For modest overpotentials, variations in partial processes are evident as inflections in the chronoamperometry and EC-MS signal. On the return step to positive potentials, hydride decomposition by H recombination to H_2 occurs in parallel with sulfate adsorption. The challenge associated with the inherent diffusional delay in the EC-MS response is mitigated by total H_2 collection and steady-state analysis facilitated by the thin-layer EC-MS cell geometry as demonstrated for the HER on a non-hydride forming Ag electrode. Analysis of the respective transients and steady-state response on Cu(111) reveals a saturated hydride fractional coverage of 0.67 at negative potentials with an upper bound charge of 106 $\mu C/cm^2$ (average electrosorption valency of ≈1.76) associated with adsorption of the $(\sqrt{3} \times \sqrt{7})$ mixed sulfate-water adlayer at positive potentials.

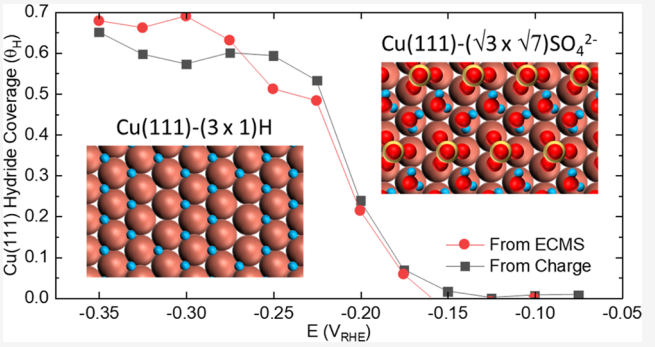

INTRODUCTION

Understanding Cu surface chemistry is of great technological interest because of its extensive use in microelectronic interconnects, along with its emergent application as the primary electrocatalyst for hydrocarbon synthesis from CO_2/CO.[1−4] In both applications, the presence and role of adsorbed H on the physical and chemical properties have yet to be fully elucidated.[5,6]

Studies of Cu(111) dosed with atomic hydrogen in ultra-high vacuum (UHV) reveal copper hydride surface phases by a combination of diffraction and spectroscopy measurements supported, more recently, by density functional theory (DFT) computations.[7−13] Beyond the low-temperature UHV setting, the formation of two-dimensional (2D) hydride on Cu(111) has also been demonstrated in acidic electrochemical environments relevant to the technical applications of interest.[14,15] Specifically, electrochemical mass spectrometry (EC-MS) combined with Raman spectroscopy indicates the formation of a 2D hydride phase on Cu(111) at potentials below the reversible potential for the H_3O^+/H_2 reaction in sulfuric acid. Unexpectedly, decomposition of the hydride phase by H recombination occurs at potentials positive of the reversible potential.[15] Similar observations of H recombination were reported for polycrystalline Cu electrodes.[16] The minimal charge transfer associated with the recombination reaction accounts for the previously unexplained voltammetric charge asymmetry associated with Cu(111) in acid media.[15] Based on H_2 evolved by recombination at positive potentials, the fractional H coverage, θ_H, relative to the metal lattice, was estimated from voltammetry to be ≈0.52 and ≈0.94 in sulfuric and perchloric acid, respectively.[15] Scanning tunneling microscopy studies of Cu(111) in sulfuric acid reveal an ordered $(\sqrt{3} \times \sqrt{7})$ sulfate adlayer at more positive potentials.[17−20] Upon stepping to more negative potentials, this gives way to (4×4) and (5×5) commensurate structures on Cu(111).[14,20] In early work, these structures were ascribed to the hydration layer[20] but subsequently were reassigned to adsorbed H.[14] Most recently, similar ordered structures were reported for water monolayers on Au(111) and Pt(111) surfaces in low-temperature UHV measurements. The long range order reflects the interactions between Eigen/Zundel hydrated protons within the adsorbed water layer, and simulations indicate that these structures remain stable although subject to thermal broadening at room temperature.[21] What role surface hydride formation may play in the structure and

Received: August 30, 2022
Revised: October 10, 2022
Published: October 21, 2022

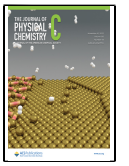

https://doi.org/10.1021/acs.jpcc.2c06207
J. Phys. Chem. C 2022, 126, 18734−18743

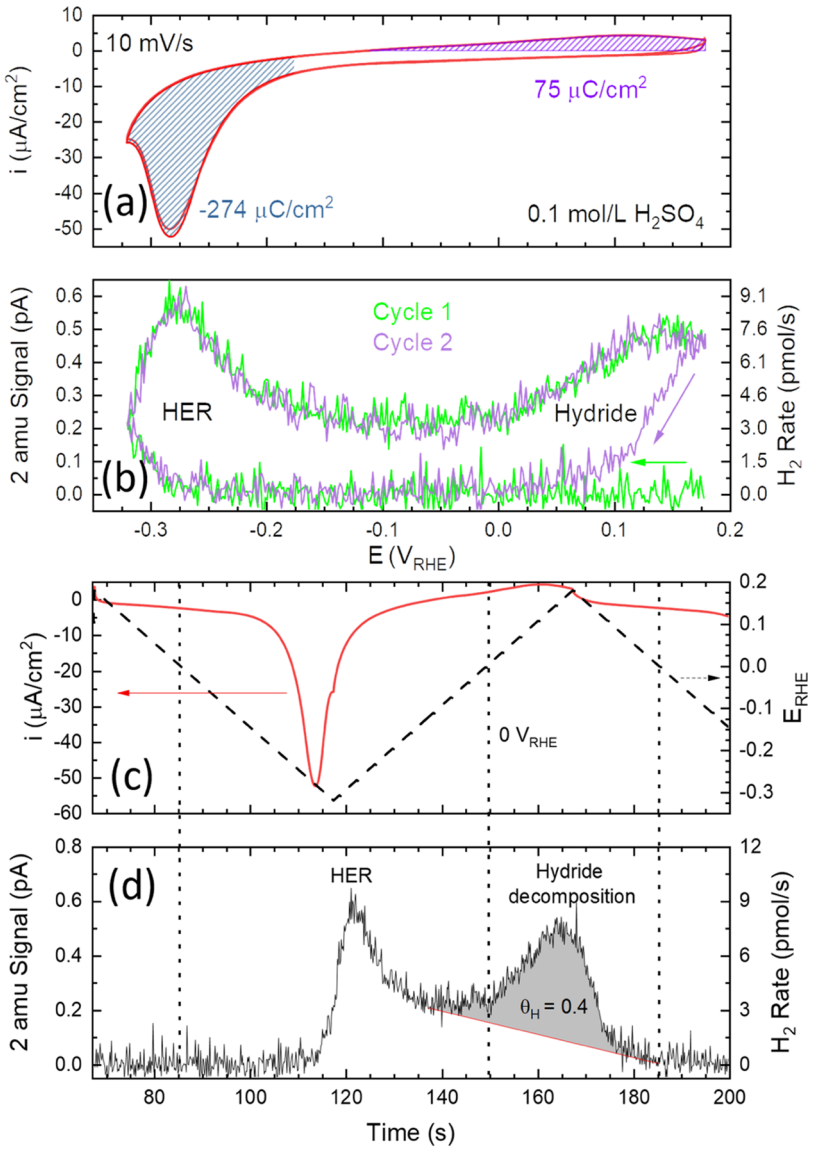

Figure 1. (a) Cyclic voltammetry with 2 complete cycles shown from 0.175 to −0.325 V_{RHE} at 10 mV/s on Cu(111) in 0.1 mol/L H_2SO_4 and (b) the corresponding 2 amu EC-MS trace. Equivalent (c) current and potential traces and (d) 2 amu EC-MS signal with time. The gray region reflects the integration performed (with a linear background) to estimate the H_2(g) generated from hydride decomposition. The dotted vertical lines spanning panels (c−d) highlight 0 V.

reactivity of such systems is a subject of long-standing interest, and there is a need for a more accurate and precise evaluation of H coverage on Cu(111) as a function of the potential.

Herein, chronoamperometry is combined with EC-MS to quantify surface hydride coverage on Cu(111) in 0.1 mol/L H_2SO_4. Hydride formation is first induced by stepping to negative potentials <0.0 V vs the reversible hydrogen electrode (RHE), where it overlaps with the hydrogen evolution reaction (HER). After a fixed period, the potential is returned to the original value >0.0 V to monitor hydride decomposition by recombination of adsorbed hydrogen (H_{ads}) to form H_2(g) while the charge associated with anion adsorption is monitored. Importantly, the small dimensions and design of the EC-MS apparatus offer the prospect of total product collection.[22] However, the diffusional lag and broadening associated with the finite thickness of the EC-MS cell limit the time resolution of the measurements. In the present work, quantitative analysis is facilitated by establishing a steady-state response for each potential of interest.[22,23] First, the correlation between the 2 amu EC-MS signal and hydrogen generation current was established by tracking the total H_2 collected during steady-state HER on a polycrystalline Ag electrode, where no hydride formation and decomposition occurs. Repeating the same procedure for experiments with Cu(111) enabled deconvolution of the potential dependence of anion desorption, hydride formation, and HER at negative potentials, followed by the inverse process of hydride decomposition by H recombination and anion adsorption at more positive potentials.

METHODS

Preparation of the Cu(111) and Polycrystalline Ag Electrode. Prior to electrochemical mass spectrometry measurements (EC-MS) both the 5 mm Cu(111) disk and 5 mm Ag disk were mechanically polished down to a 0.05 μm finish with an alumina slurry. Both disks were thoroughly rinsed and sonicated several times to remove residual alumina particles.

https://doi.org/10.1021/acs.jpcc.2c06207
J. Phys. Chem. C 2022, 126, 18734−18743

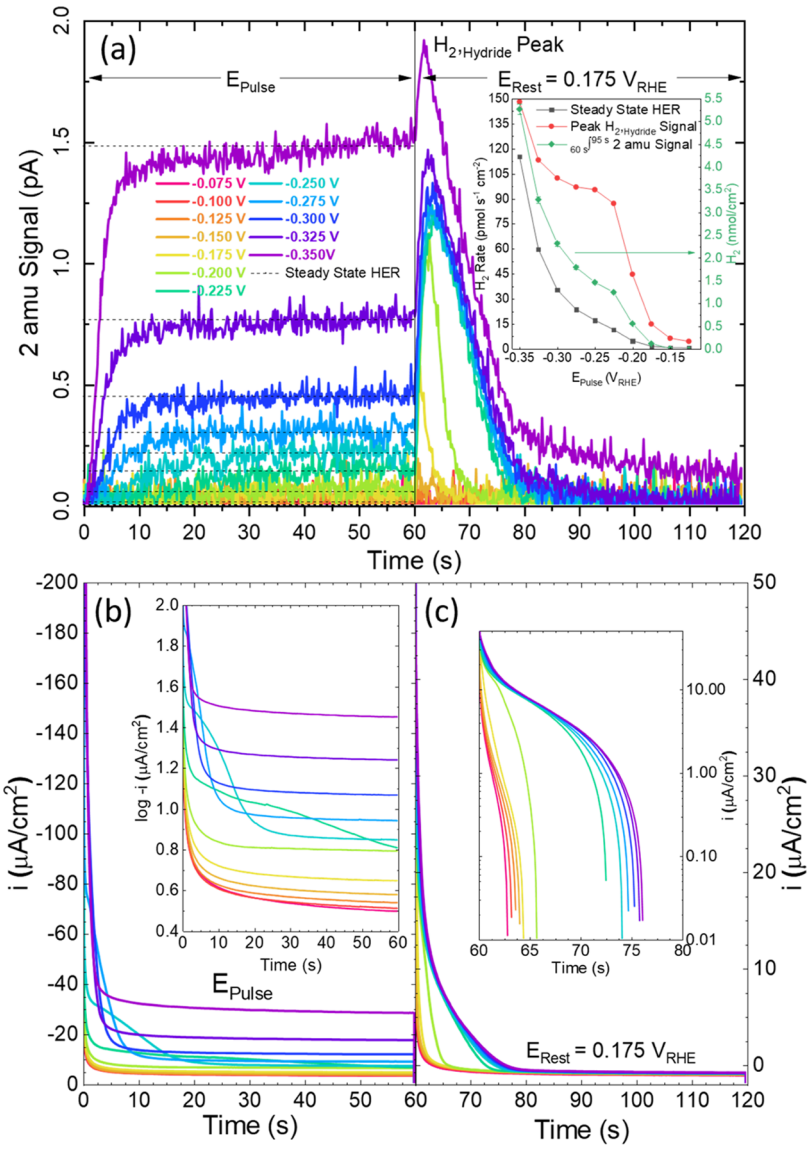

Figure 2. (a) 2 amu EC-MS signal and (b) current trace after stepping to E_{Pulse} (0 s to 60 s) and (c) after stepping back to E_{rest} (60 s to 120 s) reveal the formation of hydride on the Cu(111) surface in 0.1 mol/L H_2SO_4. The horizontal dashed black line in panel (a) is the steady-state HER rate obtained by averaging the EC-MS signal over the last 20 s of E_{pulse}. The left axis for the inset in panel (a) shows the steady-state HER rate and peak 2 amu signal associated with hydride decomposition $H_{2,hydride}$ observed at E_{rest} as a function of E_{Pulse}. The right axis for the inset shows the integrated H_2 evolved between 60 s and 95 s, which is a combination of hydride decomposition by H_{ads} recombination at E_{rest} and H_2 from HER during E_{Pulse} due to diffusional lag from the Cu(111) surface.

At this juncture, the Ag disk was dried with Ar and inserted into the EC-MS.The Cu(111) disk was treated further by electropolishing inconcentrated phosphoric acid with the Cu surface oriented facing upward, opposite from a Pt gauze electrode located approximately 6 cm away. A fixed applied of potential of 1.6 V vs the Pt counter electrode was applied for 5 min. The disk was then thoroughly rinsed with fresh 18.2 MΩ·cm H_2O, dried with Ar, and immediately mounted into the EC-MS cell.

Electrochemical Mass Spectrometry Measurements. EC-MS was performed in a thin-layer device fabricated by Spectroinlets*.[22,24] The 0.1 mol/L H_2SO_4 electrolyte was prepared afresh for each experiment using 99.999% concentrated H_2SO_4 (Sigma-Aldrich). The electrolyte was sparged with Ar through a glass frit for 1 h prior to use. The EC-MS Kel-F head was mounted with the 5 mm diameter working electrode, Ir wire counter electrode, and saturated sulfate reference electrode (SSE) in place (Figure S1). The counter and reference electrodes were in glass side arms attached to opposite sides of the cell. The Ir wire counter electrode was placed more than 3 cm away from and above the main volume of the working electrode. The electrolyte was introduced via an airtight glass syringe, followed swiftly by immediate application of 0 V vs the reversible hydrogen electrode (RHE) to mitigate oxidation and dissolution of the working electrode. During rest or idle periods between electrochemical measurements, the working electrode was likewise poised at 0 V. A Biologic SP-200 was used for all electrochemical measurements. The mass spectrometry and electrochemistry data were collected on the same computer, enabling accurate time synchronization between the two measurements. For measurements using cyclic voltammetry, the baseline of the mass spectrometry signal was subtracted via a linear baseline, where the slope was determined by averaging the spectrometry signal over 2 s before and after completion of the voltammetric scan. In the case of potential pulse measurements,

https://doi.org/10.1021/acs.jpcc.2c06207
J. Phys. Chem. C 2022, 126, 18734−18743

the baseline was zeroed via averaging the 2 amu signal for at least 2 s before initiating each E_{Pulse}.

RESULTS AND DISCUSSION

Formation of Hydride on a Cu(111) Single-Crystal Electrode. The cyclic voltammetry and the 2 amu EC-MS signal for Cu(111) in 0.1 mol/L H_2SO_4 are shown in Figure 1a,b, respectively, with a chronological representation in Figure 1c,d. The reduction peak associated with hydride formation and HER on the negative sweep, followed by decomposition of the hydride to H_2 at positive potentials on the return scan, is evident. The above processes also overlap with sulfate desorption and adsorption, respectively. An estimation of the electrochemical charge for the large reduction wave (cross-hatched region) is $-274\ \mu C/cm^2$ when the positive going sweep is taken as background (Figure 1a). In contrast, the oxidative wave yields $+75\ \mu C/cm^2$ for a fixed background of 0 A and corresponds largely to sulfate adsorption.[15,17−20] Assuming the inverse, i.e., sulfate desorption occurs during hydride formation, leaves a maximum reductive charge of $-199\ \mu C/cm^2$ available for hydride formation. This corresponds to 2.06 nmol/cm^2 of H for $n_{H.Echem}$ via eq 1, where z is the number of electrons transferred, F is Faraday's constant, and q is the net charge measured, or a fractional hydrogen surface coverage, $\theta_H = \Gamma_H/\Gamma_{Cu(111)}$ of 0.7 as referenced to the surface density of Cu(111), $\Gamma_{Cu(111)}$, of 2.935×10^{-9} mol/cm^2 (a_o, = 0.3615 nm).[25]

$$n_{H.Echem} = \frac{q}{zF} \tag{1}$$

Alternatively, the hydride coverage is estimated from the 2 amu EC-MS peak detector signal associated with hydride decomposition. Integration yields 7.5 ± 1.7 pC, based on the linear background shown in Figure 1d and the signal-to-noise ratio of the EC-MS instrument, respectively. This is converted to adsorbed hydrogen coverage, $\Gamma_{H,ECMS}$(mol H/cm^2), using eq 2 where A_{elec}(cm^2) is the geometric surface area of the electrode, q_{2amu}(C) is the integrated area of the 2 amu peak (i_{2amu}) from EC-MS, and n_{H_2} is the stoichiometry of hydride decomposition to H_2 (2 mol H/mol H_2)

$$\Gamma_{H,\ ECMS} = \frac{n_{H_2} q_{2amu}}{k_{ECMS} A_{elec}} \tag{2}$$

and $k_{ECMS}\left(\frac{C}{\text{mol } H_2}\right)$ is the spectrometry calibration factor. Calibration involved steady-state chronoamperometric analysis of the HER reaction (Figure S2a,b) for the exact same experimental configuration, adding robustness to the result. For a given potential, the current and 2 amu spectrometry signal were sampled between 50 s and 70 s and averaged. The Faradaic current was converted to the rate of H_2 produced, assuming 100% of the charge was going toward HER. The potentials used in this analysis were selected to be either more positive than hydride formation or alternatively more negative than −0.25 V to avoid overlap with sluggish hydride formation that would significantly influence the accuracy of the calibration, vide infra. The slope determined from the calibration curve, Figure S2c, is k_{ECMS} = 0.064 pC/pmol ± 0.0012 pC/pmol. The integrated EC-MS signal charge for H_2 produced from hydride decomposition, 7.5 pC ± 1.7 pC, shown in Figure 1d corresponds to an H coverage of 1.2 nmol H/cm^2 ± 0.3 nmol H/cm^2 or a fractional surface coverage, θ_H, of 0.41 ± 0.10 that stands in contrast to the 0.70 coverage derived from the voltammetric deposition charge. The discrepancy between the values determined via deposition charge versus the 2 amu EC-MS hydride decomposition signal is subject to the uncertainties associated with the background subtraction used in the respective analysis. These uncertainties are difficult to resolve due to the convolution of the EC-MS signal with delays in product transport as well as the overlap between hydride formation and the HER, not to mention the possible differences in the local HER kinetics before and after hydride formation. Furthermore, the charge analysis is incomplete as the contributions from double-layer charging and/or competitive interference from parasitic reactions such as the oxygen reduction reaction (ORR) are not addressed. A more refined approach is needed to quantify hydride surface coverage and its relationship with potential.

Chronoamperometry and EC-MS Analysis of Hydride Formation and Decomposition. Instead of sweeping the free energy as discussed above, the EC-MS 2 amu signal and charge associated with hydride formation and decomposition were examined under potentiostatic conditions by stepping the potential between a perturbation potential, E_{pulse}, and a rest potential, E_{rest} (Figure 2a). A chronological example of the potential pulse experiment is shown in Figure S3. For steady-state conditions, a sulfate-saturated Cu(111) surface is formed at the more positive "rest" potential of E_{rest} = 0.175 V.[17−20] For the first iteration between E_{pulse} and E_{rest}, E_{pulse} was set to −0.075 V for 60 s, followed by stepping back to E_{rest} for 60 s. For each successive pulse cycle, E_{pulse} was advanced to a more negative value by −25 mV. For E_{pulse} between −0.075 V and −0.150 V, minimal H_2 is measured by EC-MS during the entire potential pulse cycle (Figure 2a). At −0.175 V, a small quantity from H_2 evolution is observed at E_{pulse}, but upon switching back to E_{rest}, a sharp well-defined H_2 peak, representative of hydride decomposition ($H_{2,hydride}$), is detected and decays over ≈10 s. As E_{pulse} becomes more negative, the $H_{2,hydride}$ peak increases in both intensity and duration and appears to approach a plateau or saturation condition near −0.225 V. Stepping to more negative potentials yields a similar $H_{2,hydride}$ peak shape and intensity (relative to the baseline), as shown in the inset of Figure 2a, while stepping more negative than −0.300 V, the $H_{2,hydride}$ peak begins to increase further with accelerating contributions from potential-activated HER, as reflected by the increase in steady-state H_2 flux (e.g., at 60 s).

Integration of the $H_{2,hydride}$ decomposition peak between 60 s and 95 s yields an upper bound estimate on the H coverage (Figure 2a, green curve of inset). This upper estimate shows hydride increasing rapidly for E_{pulse} more negative than −0.175 V to reach $\theta_H \approx 0.75$ by -0.225 V. The upper bound specification arises from the diffusional lag in the EC-MS measurement that results in H_2 contributions from the preceding steady-state HER between 20 s and 60 s at E_{pulse}. In a related fashion, the subsequent rapid increase in H_2 measured at E_{rest} after E_{pulse} is advanced more negative than −0.25 V reflects the rapid acceleration of the HER and its dominant contribution to the EC-MS signal in Figure 2a, the green curve of the inset.

In tandem with EC-MS measurements, the current transients during E_{pulse} reveal an inflection associated with surface hydride formation, as shown in Figure 2b. This is most evident in the −0.225 V, −0.250 V, and −0.275 V transients, where the obscured peak current increases in magnitude while decreasing in lifetime. For −0.225 V, the steady-state current is reached within ≈50 s while for ≤0.250 V, the steady-state current is reached within ≈20 s. Replotting the respective transients (Figure S4) reveals the correlation between decay of the

https://doi.org/10.1021/acs.jpcc.2c06207
J. Phys. Chem. C 2022, 126, 18734−18743

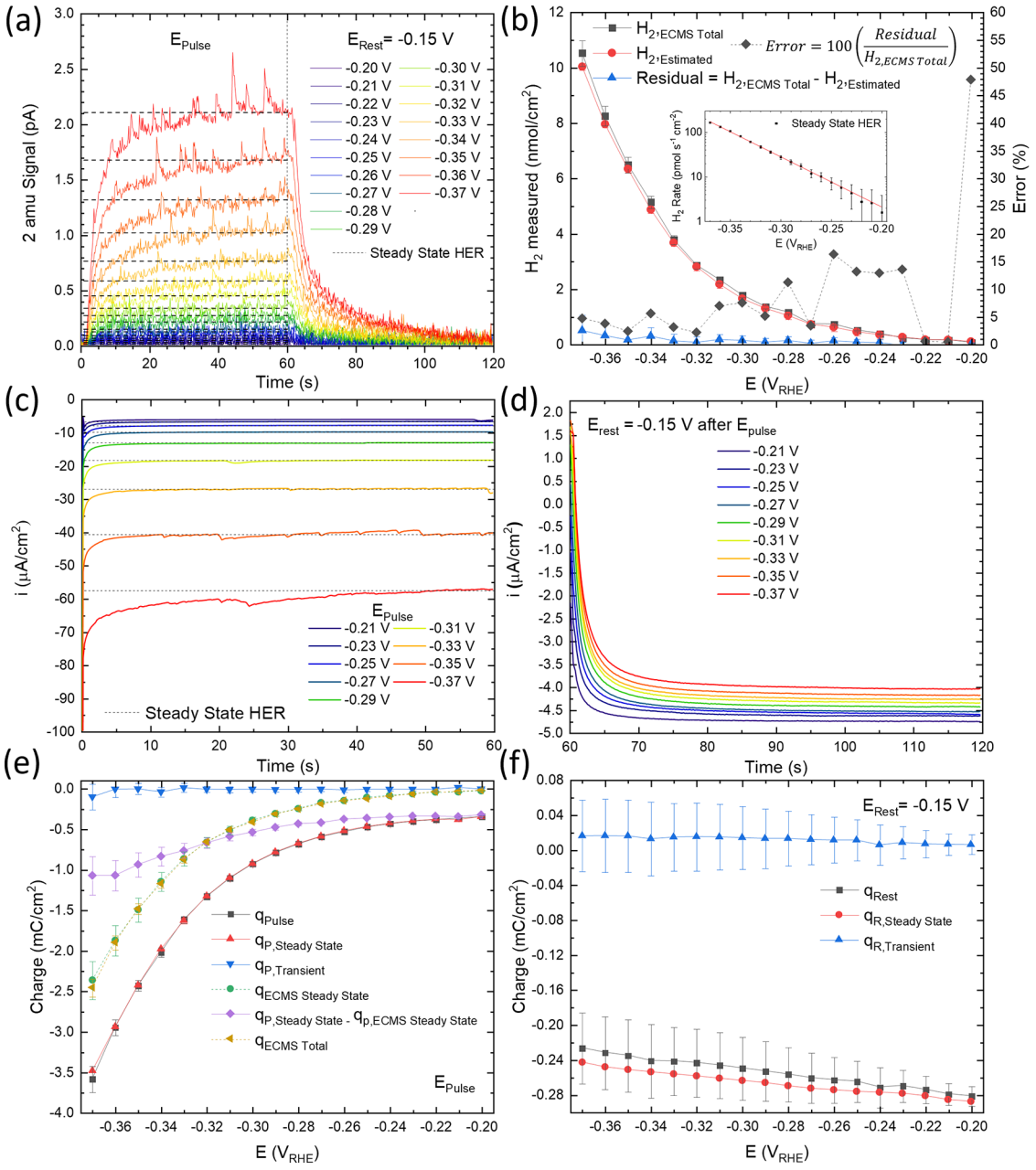

Figure 3. Potential pulse measurements on Ag configured in position 1 in 0.1 mol/L H_2SO_4. (a) 2 amu EC-MS signal for each E_{pulse} and E_{rest} sequence. (b) Comparison of total H_2 produced from the integration of the 2 amu EC-MS signal ($H_{2,ECMS\ Total}$) and that estimated from the product of the steady-state HER rate and E_{Pulse} duration ($H_{2,Estimated}$). The inset in panel (b) shows the average EC-MS signal for steady-state HER (last 20 s of the potential pulse) from which $H_{2,Estimated}$ is determined. Chronoamperometry after steeping to (c) E_{pulse} and (d) following the subsequent return to E_{rest}. The horizontal dashed lines in panel (c) represent the steady-state current (average current for the last 5 s) used to calculate the steady-state charge ($q_{P,Steady\ State}$) in panel (e). (e) Measured total charge (q_{Pulse}) compared to the calculated steady-state charge ($q_{P,Steady\ State}$) measured during E_{Pulse} (0 s to 60 s) and their difference ($q_{P,Transient}$) as well as the equivalent charge based on total H_2 detected ($q_{ECMS\ Total}$) and the steady-state HER rate from the EC-MS measurement ($q_{ECMS\ Steady\ State}$) and the difference between ($q_{Steady\ State}-q_{ECMS\ Steady\ State}$). (f) Total charge ($q_{Rest}$), steady-state charge ($q_{R,Steady\ State}$), and the difference ($q_{R,Transient}$) measured during each E_{rest} (60 s to 120 s). Note that the *x*-axis in panel (f) indicates the E_{Pulse} that preceded the step to E_{rest} with the charge being that measured during E_{rest}. Error bars represent the standard deviation of the measurements.

obscured current peak for hydride formation and the delayed rise in the 2 amu signal at E_{pulse}, subsequently followed by near saturation of the $H_{2,hydride}$ decomposition peak at E_{rest}. As E_{pulse} is advanced to more negative values, hydride formation is accelerated, and the associated coverage reaches a plateau.

Assessment of the current transients and associated charge is likewise challenging as hydride formation is accompanied by sulfate desorption and the HER. However, if hydride decomposition at E_{rest} is ascribed solely to H recombination with negligible H oxidation to hydronium, then the entire oxidative charge can be attributed to sulfate adsorption and double-layer charging.[14] The lifetime of the anion adsorption current transient closely follows that of the 2 amu hydride decomposition signal, $H_{2,hydride}$. In the absence of significant hydride formation, the current transient at E_{rest} reaches a negative parasitic background current (i.e., trace oxygen reduction) within ≈3 s. This period increases as the $H_{2,hydride}$ recombination peak increases, with background being reached

https://doi.org/10.1021/acs.jpcc.2c06207
J. Phys. Chem. C 2022, 126, 18734−18743

within ≈5 s following polarization at −0.175 V, while the value increases to ≈16 s for ≤-0.275 V, where the $H_{2,hydride}$ peak saturates as evident in Figure 2c. The difference between the net oxidative charge measured at E_{rest} after stepping from E_{Pulse} = −0.075 V vs E_{Pulse} = −0.300 V (Figure 2c) corresponds to ≈106 mC/cm^2.

Both hydride formation and sulfate desorption are correlated, strongly potential-dependent, and overlap with HER to some extent. Importantly, the transient nature of hydride formation, followed by the establishment of a steady-state H_2 evolution flux, provides an avenue for further analysis. Likewise, the inverse reaction of sulfate adsorption and hydride decomposition by H recombination, as opposed to H oxidation, not only accounts for the significant charge asymmetry in voltammetry and chronoamperometry but also provides an additional constraint on the mass/charge balance.

As detailed earlier, calibration of the EC-MS measurement involves establishing the correlation between steady-state HER current and the 2 amu signal. For the thin-layer cell, this approach yields a linear relationship between the 2 amu signal and H_2 generated, and the prospect of total product collection.[22] This capability provides an avenue for circumventing the need for a full-time domain analysis of the diffusional lag intrinsic in the EC-MS measurements.[22] Specifically, the product of the steady-state HER H_2 flux at E_{pulse} multiplied by the pulse duration yields the maximum $H_{2,HER}$ produced at the given potential and time. Any shortfall from this quantity can be attributed to hydride formation and/or anion desorption that are sampled by the 2 amu and oxidative charge, respectively, following the potential step back to E_{rest}. The viability of this approach to separate $H_{2,HER}$ and $H_{2,hydride}$ is first verified by examining the HER on Ag where surface hydride formation is absent.

Total H_2 Collection and Mass-Charge Balance for HER on Polycrystalline Ag. The premise of total H_2 collection was explored using the same potential pulse experiments on polycrystalline Ag. In contrast to Cu, the 2 amu EC-MS trace and cyclic voltammetry for Ag in 0.1 mol/L H_2SO_4 indicate the absence of hydride formation and/or decomposition, Figure S5, within the detection limit of the measurement. Accordingly, the assumption that the steady-state HER rate ($H_{2,Estimated}$) and pulse time (t_p) can be used to effectively estimate the amount of $H_{2,HER}$ produced for a given E_{pulse} can be evaluated. To explore the diffusional lag in the EC-MS measurement, three different working distances (≈140 μm, ≈200 μm, and ≈260 μm for Positions 1−3, respectively) between the Ag surface and the membrane chip were examined.[22,23] Profilometry and short impulse chronoamperometry measurements were performed to define the working distance for each configuration (Figures S6−S8), with further details available in the Supporting Material.[23] Discussion herein is focused on Position 1, which is most similar to the configuration used in the Cu experiments (compare Figures S8 and S9), vide infra.

Potential pulse measurements for each Ag disk position were performed by incrementally advancing E_{pulse} in −10 mV steps (Figures 3, S10, and S11). Integration of the 2 amu signal for each E_{pulse} (0 sto 60 s) and E_{rest} (60 s to 120 s) (Figure 3a) were summed to yield the total H_2 produced for a given pulse sequence (Figure 3b, $H_{2,ECMS\ Total}$). Like the in situ calibration pulses on Cu, a steady-state HER rate for each E_{pulse} was determined by averaging the 2 amu signal over the last 20 s of the pulse. The average rate at each E_{pulse}, dashed horizontal lines in Figure 3a (or plotted vs potential, inset Figure 3b), was multiplied by t_p (60 s) to estimate the total amount of hydrogen produced at E_{pulse} (Figure 3b, $H_{2,Estimated}$). The "Residual" or difference between $H_{2,ECMS\ Total}$ and $H_{2,Estimated}$ is constant (Figure 3b) and thus the "Error" (Residual/$H_{2,ECMS\ Total}$) in the measurement generally decreases from ≈15 % to ≈5 % as E_{pulse} becomes more negative, reflecting the larger S/N of the EC-MS signal.

Converting the $H_{2,ECMS\ Total}$ and $H_{2,Estimated}$ derived from EC-MS to charge, $q_{ECMS\ Total}$, and $q_{ECMS\ Steady\ State}$, respectively (Table 1), enables comparison to the charge from chronoamperometric data (Figure 3c,d). Integration of the 60 s E_{pulse} current transients (i_{EC}) is denoted as q_{Pulse} (black squares) while approximation of the charge based on the product of the steady-state current density (Figure 3c) and pulse time (t_p) is given as $q_{P,Steady\ State}$ (red triangles, Figure 3e). As evident in Figure 3c,d, the steady-state currents are reached <5 s after applying E_{pulse} or E_{rest}, respectively, such that the difference between q_{Pulse} and $q_{P,Steady\ State}$ shown in Figure 3e is negligible and falls within the standard deviation of the measurement. However, a comparison to the charge derived from the steady-state approximation of the EC-MS measurement, $q_{ECMS\ Steady\ State,}$ reveals an offset of −0.5 mC/cm^2 at more positive pulse potentials that increases to −1 mC/cm^2 by −0.37 V. The offset primarily reflects the charge consumed by parasitic ORR, which is also present in the steady-state charge measured during E_{rest}, $q_{R,Steady\ State}$ (Figure 3f). The ≥1 mC/cm^2 offset between EC-MS approximation and charge measured is somewhat analogous to the zero-point offset in the steady-state current—2 amu EC-MS signal calibration, although it helpfully reveals the potential dependence of the parasitic background process (see the Supporting Material for a more detailed discussion). Experiments with the other two Ag positions show similar offsets but with a weaker dependence on E_{pulse} (Figures S10e and S11e). Applying a similar analysis to

Table 1. Symbol Definitions

parameter	units	definition
θ_H	$\Gamma_H/\Gamma_{Cu(111)}$	fractional H coverage on Cu(111) per Cu atom basis
E_{pulse}	V	pulse potential, t = 0−120 s
E_{rest}	V	rest potential, t = 60−120 s
$H_{2,ECMS\ Total}$	nmol/cm^2	$\frac{k_{ECMS}}{A_{elec}}\int_0^{120} i_{2amu}(E,t)dt$
$H_{2,estimated} = H_{2,HER}$	nmol/cm^2	$\frac{k_{ECMS} t_P}{A_{elec}} \bar{i}_{2amu,t\ =\ 40\ s \rightarrow 60\ s}$
$H_{2,hydride}$	nmol/cm^2	$H_{2,ECMS\ total} - H_{2,HER}$
$q_{ECMS\ total}$	C/cm^2	$\frac{zFH_{2,ECMS\ total}}{A_{elec}}$
$q_{ECMS\ steady\ state}$	C/cm^2	$\frac{zFH_{2,HER}}{A_{elec}}$
q_{pulse}	C/cm^2	$A_{elec}^{-1}\int_0^{60} i_{EC}(E,t)dt$
q_{rest}	C/cm^2	$A_{elec}^{-1}\int_{60}^{120} i_{EC}(E,t)dt$
$q_{P,steady\ state}$	C/cm^2	$\frac{t_P}{A_{elec}} \bar{i}_{EC,t\ =40\ s \rightarrow 60\ s}$
$q_{R,steady\ state}$	C/cm^2	$\frac{t_R}{A_{elec}} \bar{i}_{EC,t\ =100\ s \rightarrow 120\ s}$
$q_{P,transient}$	C/cm^2	$q_{Pulse} - q_{P,steady\ state}$
$q_{R,transient}$	C/cm^2	$q_{Rest} - q_{T,steady\ state}$
$q_{P,Tafel}$	C/cm^2	$\frac{t_P}{A_{elec}}(0.0089E_{pulse} + 0.0037)$, see Figure S13
$q_{P,transient\ (Tafel)}$	C/cm^2	$q_{Pulse} - q_{P,Tafel}$
$H_{2,hydride}(q_{transient})$	nmol/cm^2	$\frac{q_{P,transient} - q_{R,transient}}{zF}$ or $\frac{q_{P,transient\ (Tafel)} - q_{R,transient}}{zF}$

https://doi.org/10.1021/acs.jpcc.2c06207
J. Phys. Chem. C 2022, 126, 18734−18743

the oxidation transient(s), Figure 3d, reveals the effectiveness of the steady-state approximation, albeit dominated by parasitic background processes. The above analysis, combined with the voltammetry shown in Figure S5, points to a negligible contribution of H_2 oxidation.

Quantifying Hydride Coverage on Cu(111) from Potential Pulse Experiments. With the total H_2 collection experiments on Ag supporting the steady-state approximation of the rate of HER (i.e., $H_{2,HER} \approx H_{2,Estimated}$), quantification of the more complex EC-MS $H_{2,hydride}$ response (Figure 4a) and charge transient associated with hydride formation on Cu(111) is examined in more detail. The $H_{2,HER}$ evaluated from the steady-state EC-MS HER rate at E_{pulse} (dashed horizontal lines, Figure 2a) was subtracted from measured $H_{2,ECMS\ Total}$ during a given pulse sequence to generate a residual, ascribed to $H_{2,hydride}$ (Figure 4a), that exhibits a sigmoidal dependence on potential. The so-derived $H_{2,hydride}$ is less than that associated with the integration of the measured H_2 from 60 s and 90 s (Figure 2a, inset) due to contributions from the HER associated with diffusional lag in the spectrometer. This is well demonstrated by EC-MS impulse experiments, Figure S9, where the time frame of the diffusional lag associated with H_2 from the HER occurs over 15 s after the pulse. By this subtractive analysis, a significant quantity of hydride is first detected at −0.175 V (Figure 4a). The hydride coverage increases substantially with decreasing E_{pulse} and reaches saturation near 1 nmol/cm^2 of H by −0.275 V. The saturation plateau from−0.275 V to −0.350 V equates to two-thirds fractional H surface coverage, $\theta_H \approx 0.67$, on Cu(111). This coverage is maintained even when the pulse time is increased to 90 s (Figure 4a, inset). Extending the E_{pulse} duration enables saturation to be reached at −0.225 V, that is, between 25 mV to 50 mV more positive than that observed for 60 s pulses. Likewise, varying the duration of E_{pulse} between 15 s and 90 s leads to variation in the amount of hydride formed between −0.175 V and −0.225 V (Figure 4a, inset).

Interestingly, over the same potential range where hydride formation is dependent on pulse time, the (pseudo) steady-state HER rate measured by EC-MS is partially dependent on pulse time within the standard deviations of the measurements. Ignoring the results for 5 s, the steady-state HER rates at intermediate potentials are plotted on a log scale (Figure S12). At −0.2 V, a positive correlation between average HER rate and pulse time is evident and perhaps even clearer at −0.225 V. The time dependence of the average HER rate diminishes for $E_{pulse} \leq$ 0.25 V, congruent with the more rapid completion of hydride formation and sulfate desorption. It will be challenging to determine if the hydride coverage impact on the HER kinetics reflects the properties of the hydride phase itself or is primarily due to the removal of the blocking sulfate adlayer. Experiments performed in a different electrolyte may offer more insight into this question.

Upon stepping to E_{rest}, hydride decomposition by H_{ads} recombination to H_2 occurs rather than its removal by oxidation to hydronium. This enables the charge associated with SO_4^{2-} adsorption, $q_{R,Transient}$, (Figure 4b) to be estimated by subtracting the integrated parasitic steady-state background current, $q_{R,Steady\ State}$, from the total integrated charge, q_{Rest}. As with the Ag control experiment, the charge from the steady-state current is negative due to parasitic ORR, and, in this analysis, its rate is assumed to be independent of the evolution of the hydride/SO_4^{2-} coverage. When E_{pulse} is between −0.075 V and −0.150 V, the transient charge, $q_{R,Transient}$, increases minimally from 20 μC/cm^2 to 25.9 μC/cm^2. However, as E_{pulse} is advanced from −0.150

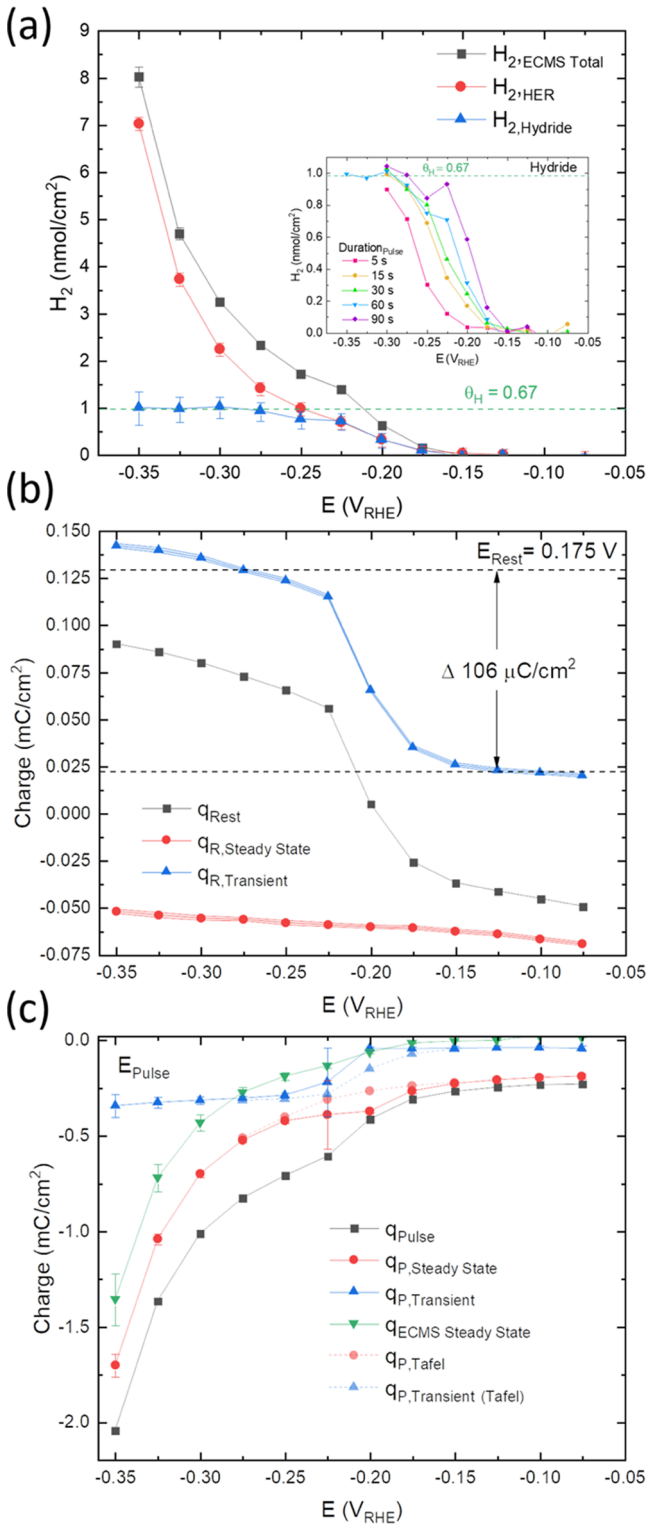

Figure 4. (a) Hydride coverage on Cu(111) determined by deconvolution of the 2 amu EC-MS signal for $H_{2,HER}$ from the $H_{2,EC\text{-}MS\ Total}$ for the potential pulse experiments in Figure 2. The inset depicts the dependence of hydride formation on the duration of E_{Pulse}. (b−c) Integration and comparison of current transients for (b) anion adsorption upon stepping to E_{rest} (60 s to 120 s) and (c) for anion desorption and hydride formation upon stepping to E_{pulse} (0 s to 60 s). Note that the *x*-axis in panel (b) indicates the potential of the E_{Pulse} preceding E_{rest}, with the reported charge being that measured at E_{rest}. The notation "Tafel" represents a subsequent evaluation of the respective charge by Tafel slope extrapolation to estimate the steady-

https://doi.org/10.1021/acs.jpcc.2c06207
J. Phys. Chem. C 2022, 126, 18734−18743

Figure 4. continued

state $H_{2,HER}$ current during E_{pulse}, as shown in Figure S13. The line width in panel (b) and error bars in panels (a, c) represent the standard deviation of the measurements.

V to −0.225 V, $q_{R,Transient}$ increases substantially to 115 $\mu C/cm^2$ and eventually reaches 142 $\mu C/cm^2$ by −0.350 V. Given the saturation conditions for hydride formation from the EC-MS signal is reached by −0.275 V, the difference in charge, ≈Δ106 $\mu C/cm^2$, between −0.300 V and −0.125 V is attributed to SO_4^{2-} adsorption. The assignment aligns well with previous Raman studies, indicating the formation of saturated sulfate adlayers on Cu(111)[15,26,27] under these conditions. Likewise, ECSTM studies reveal the adlayer adopts a $(\sqrt{3} \times \sqrt{7})$ structural variant with a longer-range Moire pattern as a result of superposition with the reconstructed Cu(111) surface.[14,17−20] Consistent with the overlayer structure, a radiotracer study indicates a fractional coverage of $\theta_{SO_4} \approx 0.21$ on Cu(111).[28] An upper bound estimate of the charge based on compensation of the valence of the solvated sulfate species would be 120 $\mu C/cm^2$, which compares to the measured value of ≈Δ106 $\mu C/cm^2$. This corresponds to an electrosorption valency of 1.76, similar to that reported for $(\sqrt{3} \times \sqrt{7})$ sulfate adlayers on other 111 fcc surfaces.[29−31]

Inverse analysis based on reversibility of sulfate adsorption enables deconvolution of the charge $q_{P,Transient}$ associated with hydride formation at E_{pulse}. The potential dependence of $q_{P,Transient}$ is like that for $H_{2,hydride}$ determined from EC-MS, as shown in Figure 4c, although the transition of $q_{P,Transient}$ to saturation occurs more abruptly. A significant $q_{P,Transient}$ charge is first observed at −0.225 V and saturates by −0.250 V at ≈−275 $\mu C/cm^2$ (Figures 4c and 5a), whereas the EC-MS data shows hydride formation begins at potentials as positive as −175 mV. This discrepancy is likely due to the slow rate of hydride formation at smaller overpotentials (Figures 2b and S4) that results in significant overlap with the steady-state HER current leading to an overestimate of the latter. To explore this further, a Tafel plot was generated using the steady-state current from Figure 2. The current density at the four most negative pulse potentials, where hydride saturation is achieved, were used to find the Tafel slope (Figure S13). Extrapolation to lower overpotentials was used to predict the charge associated with HER at E_{pulse} from −0.175 V to −0.250 V ($q_{P,Tafel}$ in Figure 4c). The difference between $q_{P,Steady\ State}$ and $q_{P,Tafel}$ represents the incremental charge contribution associated with sulfate desorption and hydride formation. Adding this to $q_{P,Transient}$ at intermediate potentials generates $q_{P,Transient\ (Tafel)}$ in Figure 5a, which shows a much more gradual rise in sulfate desorption/hydride formation with potential that is more congruent with the relationship between potential and hydride formation measured by EC-MS (Figure 4a) and the adsorption of sulfate with the return step to E_{rest} (Figure 4b). In fact, if sulfate desorption is assumed to be equal and opposite to $q_{R,Transient}$ for its adsorption, then the remaining charge in $q_{P,Transient\ (Tafel)}$ can be ascribed predominantly to hydride formation. Converting this charge to H_2 ($H_{2,Hydride}$ ($q_{Transient}$)) and comparing this result with the inverse decomposition process, i.e., $H_{2,hydride}$ from the EC-MS measurement, captures the plausibility of this inference (Figure 5b).

Finally, the difference in $q_{P,Transient}$ between −0.300 and −0.125 mV (275 mC/cm^2) captures complete sulfate desorption and hydride formation. As the saturated sulfate coverage for adsorption at E_{rest} was determined to be 106 mC/cm^2 in Figure 4c, this leaves 169 mC/cm^2 for hydride formation. This converts to θ_H of 0.6 on Cu(111), close to the coverage measured by EC-MS (Figures 4c and 5b).

Chemisorption of hydrogen on Cu(111) in UHV has been studied using high-resolution electron energy loss spectroscopy.[7,11] Loss peaks at 100 meV (806. 6 cm^{-1}) and 129 meV (1040.46 cm^{-1}) were measured at H coverages below 0.5 and assigned to binding at 3-fold hollow sites. The assignment was congruent with a subsequent infrared reflection absorption spectroscopy study, although this differed from earlier work on the topic.[8,10] At higher coverages, a third loss peak was measured at 115 meV (927.5 cm^{-1}) that was assigned to subsurface hydrogen that begins to form as occupancy of the 3-fold hollow sites begins to approach saturation. More recently, DFT indicated that 3-fold hollow surface sites are preferred over subsurface sites for $\theta_H < 0.67$.[12] At higher coverages, the

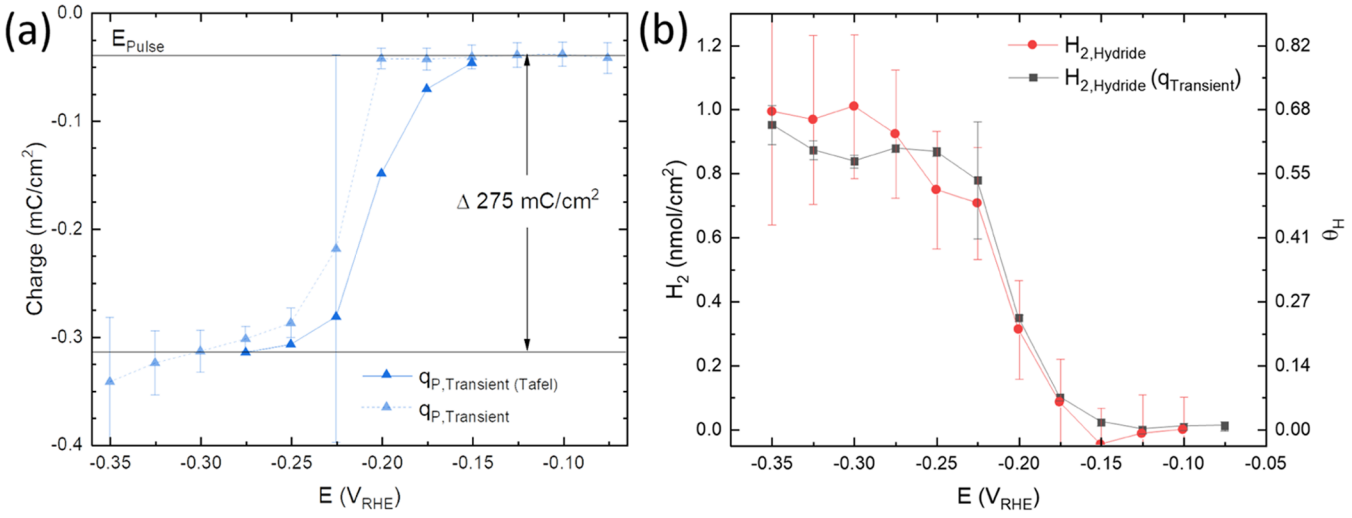

Figure 5. (a) Transient charge measured during anion desorption and hydride formation at E_{Pulse} before ($q_{P,Transient}$) and after adjustment via the Tafel fit ($q_{P,Transient\ (Tafel)}$) in Figure S13. (b) $H_{2,hydride}$ determined from the EC-MS signal compared to that from $q_{P,Transient\ (Tafel)}$ ($H_{2,Hydride}$ ($q_{Transient}$)) after subtracting the charge from sulfate adsorption during E_{Rest} ($q_{R,Transient}$). Error bars represent the standard deviation of the measurement.

https://doi.org/10.1021/acs.jpcc.2c06207
J. Phys. Chem. C 2022, 126, 18734−18743

presence of hydrogen at adjacent fcc and hcp sites increases the surface adsorption potential such that the adsorption at subsurface sites eventually becomes more favorable.[12] Calculations also indicate that the energy for H adsorption to hcp sites is isoenergetic relative to binding at fcc sites.[13] Calculations evaluating overpotential adsorption of hydrogen on Cu (111) indicate that the H_{ads} adsorption energy decreases with potential and increasing coverage, with a marked increase in the HER occurring near −0.4 V SHE corresponding to a coverage, in excellent agreement with the present results.[32] The 0.67 fractional H coverage observed for the potential and electrolyte conditions reported herein supports H binding to three-fold hollow sites on Cu(111) and the (3 × 1) structure suggested by DFT[12] that with multiple domains would be congruent with the (3 × 3) LEED results.[8] Hydride formation and decomposition are strongly potential-dependent and coupled with anion desorption and adsorption, respectively. It is possible that at more negative potentials or other electrolyte compositions, different coverages or structural configurations of the hydride might be possible. It remains to be determined how the hydride phase, i.e., (3 × 3) comprised of (3 × 1) like domains, interacts with hydronium and other cations to render the interesting $c(4 \times 4)$ and $c(5 \times 5)$ structures reported in scanning tunneling microscopy studies.[14,20,21]

The importance of H_{ads} in electrocatalytic hydrogenation reactions, such as CO_2 reduction to hydrocarbon and oxygenates on Cu surfaces, are just beginning to be explored. The present results provide new insights and further motivation to examine the role of H_{ads} in guiding the selectivity and efficiency of hydrogenation reactions, in ways that may be analogous to prior work in homogeneous catalysis involving Cu−H bonds.[33,34] Likewise, these results provide hints as to the possible role of proton reduction and hydride formation in the electrodeposition of Cu at high overpotentials, along with the impact of H on microstructural evolution.[35,36]

CONCLUSIONS

EC-MS is combined with chronoamperometry to quantify the H surface coverage associated with the hydride surface phase formed on Cu(111) in sulfuric acid electrolyte. Control experiments on a non-hydride forming Ag surface were used to demonstrate the utility of the steady-state approximation to determine the total H_2 produced from HER in the thin-layer EC-MS cell. The total H_2 collection capability of the EC-MS apparatus enables the mass and charge associated with hydride formation or decomposition by H recombination and associated anion desorption or adsorption on Cu(111) to be studied in detail. At negative potentials, desorption of the sulfate adlayer is coincident with the formation of the surface hydride. The hydride has a fractional surface coverage θ_H of 0.67 relative to the Cu(111) surface congruent with H occupying the three-fold hollow sites. Modifying the amount of copper hydride formed via pulse time revealed that the steady-state HER rate was positively correlated to the degree of surface hydride and/or inversely related to adsorbed sulfate. Hydride decomposition proceeds by H_{ads} recombination rather than oxidation such that the majority of the oxidation charge can be associated with the formation of the $(\sqrt{3} \times \sqrt{7})$ mixed sulfate-water adlayer.

ASSOCIATED CONTENT

Supporting Information

The Supporting Information is available free of charge at https://pubs.acs.org/doi/10.1021/acs.jpcc.2c06207.

Detailed discussion of profilometry measurements; calibration of the EC-MS instrument, determination of electrode position via profilometry and impulse measurements; and influence of parasitic ORR in Ag and Cu potential pulse measurements; depicting calibration of the EC-MS instrument, potential pulse experiment, the relationship between current and EC-MS signal; integrated EC-MS signal during the rest potential period of the pulsing sequence; cyclic voltammetry, and corresponding EC-MS signal for polycrystalline Ag; optical pictures of the EC-MS electrochemical cell and 2D/3D profilometry of the three electrode positions; 3D maps of height differences between working electrode positions; impulse measurements and simulations of impulse measurements on Ag and Cu; results of potential pulse measurements for Ag in electrode positions 2 and 3,; average steady-state hydrogen evolution on Ag in position 1; chronoamperometry during pulse measurements for Ag in position 1; dependence of hydride formation and hydride formation on Cu(111) with variation in potential pulse time, and Tafel slope fitted to steady-state HER current on Cu(111) (PDF)

AUTHOR INFORMATION

Corresponding Authors

David Raciti − *Materials Science and Engineering Division, National Institute of Standards and Technology, Gaithersburg, Maryland 20899, United States;* orcid.org/0000-0002-9580-4524; Email: david.raciti@nist.gov

Thomas P. Moffat − *Materials Science and Engineering Division, National Institute of Standards and Technology, Gaithersburg, Maryland 20899, United States;* orcid.org/0000-0003-4377-1692; Email: thomas.moffat@nist.gov

Complete contact information is available at: https://pubs.acs.org/10.1021/acs.jpcc.2c06207

Notes

The authors declare no competing financial interest.

*Certain commercial equipment, instruments, or materials are identified in this paper to specify the experimental procedure adequately. Such identification is not intended to imply recommendation or endorsement by the National Institute of Standards and Technology, nor is it intended to imply that the materials or equipment identified are necessarily the best available for the purpose.

ACKNOWLEDGMENTS

The authors thank Nicole Ritzert for assistance with profilometry measurements.

REFERENCES

(1) Moffat, T. P.; Wheeler, D.; Edelstein, M. D.; Josell, D. Superconformal Film Growth: Mechanism and Quantification. *IBM J. Res. Dev.* **2005**, *49*, 19−36.

(2) Nitopi, S.; Bertheussen, E.; Scott, S. B.; Liu, X.; Engstfeld, A. K.; Horch, S.; Seger, B.; Stephens, I. E. L.; Chan, K.; Hahn, C.; et al. Progress and Perspectives of Electrochemical CO_2 Reduction on Copper in Aqueous Electrolyte. *Chem. Rev.* **2019**, *119*, 7610−7672.

(3) Raciti, D.; Braun, T. M.; Hight Walker, A. R.; Moffat, T. P. Mapping Surface Chemistry During Superfilling with Shell-Isolated Nanoparticle Enhanced Raman Spectroscopy and X-Ray Photoelectron Spectroscopy. *J. Electrochem. Soc.* **2022**, *169*, No. 082506.

(4) Raciti, D.; Wang, C. Recent Advances in CO2 Reduction Electrocatalysis on Copper. *ACS Energy Lett.* **2018**, *3*, 1545−1556.
(5) Ceyer, S. T. The Unique Chemistry of Hydrogen beneath the Surface: Catalytic Hydrogenation of Hydrocarbons. *Acc. Chem. Res.* **2001**, *34*, 737−744.
(6) Fukumuro, N.; Adachi, T.; Yae, S.; Matsuda, H.; Fukai, Y. Influence of Hydrogen on Room Temperature Recrystallisation of Electrodeposited Cu Films: Thermal Desorption Spectroscopy. *Trans. IMF* **2011**, *89*, 198−201.
(7) Lee, G.; Plummer, E. W. High-Resolution Electron Energy Loss Spectroscopy Study on Chemisorption of Hydrogen on Cu(111). *Surf. Sci.* **2002**, *498*, 229−236.
(8) Mccash, E. M.; Parker, S. F.; Pritchard, J.; Chesters, M. A. The Adsorption of Atomic Hydrogen on Cu(111) Investigated by Reflection-Absorption Infrared Spectroscopy, Electron Energy Loss Spectroscopy and Low Energy Electron Diffraction. *Surf. Sci.* **1989**, *215*, 363−377.
(9) Mudiyanselage, K.; Yang, Y.; Hoffmann, F. M.; Furlong, O. J.; Hrbek, J.; White, M. G.; Liu, P.; Stacchiola, D. J. Adsorption of Hydrogen on the Surface and Sub-Surface of Cu(111). *J. Chem. Phys.* **2013**, *139*, No. 044712.
(10) Lamont, C. L. A.; Persson, B. N. J.; Williams, G. P. Dynamics of Atomic Adsorbates: Hydrogen on Cu(111). *Chem. Phys. Lett.* **1995**, *243*, 429−434.
(11) Greuter, F.; Ward Plummer, E. Chemisorption of Atomic Hydrogen on Cu(111). *Solid State Commun.* **1983**, *48*, 37−41.
(12) Luo, M.; Hu, G. Coverage-dependent absorption of atomic hydrogen into the sub-surface of Cu(111) studied by density-functional-theory calculations. *Surf. Sci.* **2009**, *603*, 1081−1086.
(13) Xu, L.; Lin, J.; Bai, Y.; Mavrikakis, M. Atomic and Molecular Adsorption on Cu(111). *Top. Catal.* **2018**, *61*, 736−750.
(14) Huynh, T. M. T.; Broekmann, P. From In Situ towards In Operando Conditions: Scanning Tunneling Microscopy Study of Hydrogen Intercalation in Cu(111) during Hydrogen Evolution. *ChemElectroChem* **2014**, *1*, 1271−1274.
(15) Tackett, B. M.; Raciti, D.; Walker, A. R. H.; Moffat, T. P. Surface Hydride Formation on Cu(111) and Its Decomposition to Form H2 in Acid Electrolytes. *J. Phys. Chem. Lett.* **2021**, *12*, 10936−10941.
(16) Scott, S. B.; Engstfeld, A. K.; Jusys, Z.; Hochfilzer, D.; Knøsgaard, N.; Trimarco, D. B.; Vesborg, P. C. K.; Behm, R. J.; Chorkendorff, I. Anodic Molecular Hydrogen Formation on Ru and Cu Electrodes. *Catal. Sci. Technol.* **2020**, *10*, 6870−6878.
(17) Li, W.-H.; Nichols, R. J. An in Situ STM Study of Sulphate Adsorption on Copper(111) in Acidic Aqueous Electrolytes. *J. Electroanal. Chem.* **1998**, *456*, 153−160.
(18) Broekmann, P.; Wilms, M.; Kruft, M.; Stuhlmann, C.; Wandelt, K. In-Situ STM Investigation of Specific Anion Adsorption on Cu(111). *J. Electroanal. Chem.* **1999**, *467*, 307−324.
(19) Broekmann, P.; Wilms, M.; Spaenig, A.; Wandelt, K. Morphological Aspects of Sulfate-Induced Reconstruction of Cu(111) in Sulfuric Acid Solution: In Situ STM Study. *Prog. Surf. Sci.* **2001**, *67*, 59−77.
(20) Broeckmann, P.; Wilms, M.; Arenz, M.; Spänig, A.; Wandelt, K.Atomic Structure of Cu(111) Surfaces in Dilute Sulfuric Acid Solution. In *Solid—Liquid Interfaces: Macroscopic Phenomena—Macroscopic Understanding*; Wandelt, K.; Thurgate, S. Eds.; Springer: Berlin, Heidelberg, 2003; pp 141−199.
(21) Tian, Y.; Hong, J.; Cao, D.; You, S.; Song, Y.; Cheng, B.; Wang, Z.; Guan, D.; Liu, X.; Zhao, Z.; et al. Visualizing Eigen/Zundel Cations and Their Interconversion in Monolayer Water on Metal Surfaces. *Science* **2022**, *377*, 315−319.
(22) Trimarco, D. B.; Scott, S. B.; Thilsted, A. H.; Pan, J. Y.; Pedersen, T.; Hansen, O.; Chorkendorff, I.; Vesborg, P. C. K. Enabling Real-Time Detection of Electrochemical Desorption Phenomena with Sub-Monolayer Sensitivity. *Electrochim. Acta* **2018**, *268*, 520−530.
(23) Krempl, K.; Hochfilzer, D.; Scott, S. B.; Kibsgaard, J.; Vesborg, P. C. K.; Hansen, O.; Chorkendorff, I. Dynamic Interfacial Reaction Rates from Electrochemistry−Mass Spectrometry. *Anal. Chem.* **2021**, *93*, 7022−7028.
(24) Trimarco, D. B.; Pedersen, T.; Hansen, O.; Chorkendorff, I.; Vesborg, P. C. K. Fast and Sensitive Method for Detecting Volatile Species in Liquids. *Rev. Sci. Instrum.* **2015**, *86*, No. 075006.
(25) Straumanis, M. E.; Yu, L. S. Lattice Parameters, Densities, Expansion Coefficients and Perfection of Structure of Cu and of Cu−In α Phase. *Acta Crystallogr., Sect. A* **1969**, *25*, 676−682.
(26) Bodappa, N.; Su, M.; Zhao, Y.; Le, J.-B.; Yang, W.-M.; Radjenovic, P.; Dong, J.-C.; Cheng, J.; Tian, Z.-Q.; Li, J.-F. Early Stages of Electrochemical Oxidation of Cu(111) and Polycrystalline Cu Surfaces Revealed by in Situ Raman Spectroscopy. *J. Am. Chem. Soc.* **2019**, *141*, 12192−12196.
(27) Brown, G. M.; Hope, G. A. In-Situ Spectroscopic Evidence for the Adsorption of SO2−4 Ions at a Copper Electrode in Sulfuric Acid Solution. *J. Electroanal. Chem.* **1995**, *382*, 179−182.
(28) Smoliński, S.; Sobkowski, J. Adsorption of Sulfate Ions on Monocrystalline Copper Electrodes: The Structural Effects. *J. Electroanal. Chem.* **1999**, *463*, 1−8.
(29) Kolics, A.; Wieckowski, A. Adsorption of Bisulfate and Sulfate Anions on a Pt(111) Electrode. *J. Phys. Chem. B* **2001**, *105*, 2588−2595.
(30) Gossenberger, F.; Juarez, F.; Groß, A. Sulfate, Bisulfate, and Hydrogen Co-Adsorption on Pt(111) and Au(111) in an Electrochemical Environment. *Front. Chem.* **2020**, *8*, No. 634.
(31) Comas-Vives, A.; Bandlow, J.; Jacob, T. Ab Initio Study of the Electrochemical H2SO4/Pt(111) Interface. *Phys. Chem. Chem. Phys.* **2013**, *15*, 992−997.
(32) Zhao, M.; Anderson, A. B. Theory of Hydrogen Deposition and Evolution on Cu(111) Electrodes. *J. Electrochem. Soc.* **2017**, *164*, H691−H695.
(33) Liu, R. Y.; Buchwald, S. L. CuH-Catalyzed Olefin Functionalization: From Hydroamination to Carbonyl Addition. *Acc. Chem. Res.* **2020**, *53*, 1229−1243.
(34) Deutsch, C.; Krause, N.; Lipshutz, B. H. CuH-Catalyzed Reactions. *Chem. Rev.* **2008**, *108*, 2916−2927.
(35) Yoshida, H.; Yamazaki, T.; Adachi, T.; Fukumuro, N.; Yae, S.; Fukai, Y. Hydrogen-Induced Grain Growth in Electrodeposited Cu Films. *J. Jpn. Inst. Met. Mater.* **2015**, *79*, 78−81.
(36) Yin, D.; Murdoch, H. A.; Hornbuckle, B. C.; Hernández-Rivera, E.; Dunstan, M. K. Investigation of Anomalous Copper Hydride Phase during Magnetic Field-Assisted Electrodeposition of Copper. *Electrochem. Commun.* **2019**, *98*, 96−100.

https://doi.org/10.1021/acs.jpcc.2c06207
J. Phys. Chem. C 2022, 126, 18734−18743